

Two-particle correlations on transverse momentum and minijet dissipation in Au-Au collisions at $\sqrt{s_{NN}} = 130$ GeV

J. Adams,³ M.M. Aggarwal,²⁹ Z. Ahammed,⁴⁴ J. Amonett,²⁰ B.D. Anderson,²⁰ D. Arkhipkin,¹³ G.S. Averichev,¹² S.K. Badyal,¹⁹ Y. Bai,²⁷ J. Balewski,¹⁷ O. Barannikova,³² L.S. Barnby,³ J. Baudot,¹⁸ S. Bekele,²⁸ V.V. Belaga,¹² A. Bellingeri-Laurikainen,³⁹ R. Bellwied,⁴⁷ J. Berger,¹⁴ B.I. Bezverkhny,⁴⁹ S. Bharadwaj,³⁴ A. Bhasin,¹⁹ A.K. Bhati,²⁹ V.S. Bhatia,²⁹ H. Bichsel,⁴⁶ J. Bielcik,⁴⁹ J. Bielcikova,⁴⁹ A. Billmeier,⁴⁷ L.C. Bland,⁴ C.O. Blyth,³ S-L. Blyth,²¹ B.E. Bonner,³⁵ M. Botje,²⁷ A. Boucham,³⁹ J. Bouchet,³⁹ A.V. Brandin,²⁵ A. Bravar,⁴ M. Bystersky,¹¹ R.V. Cadman,¹ X.Z. Cai,³⁸ H. Caines,⁴⁹ M. Calderón de la Barca Sánchez,¹⁷ J. Castillo,²¹ O. Catu,⁴⁹ D. Cebra,⁷ Z. Chajecki,²⁸ P. Chaloupka,¹¹ S. Chattopadhyay,⁴⁴ H.F. Chen,³⁷ J.H. Chen,³⁸ Y. Chen,⁸ J. Cheng,⁴² M. Cherney,¹⁰ A. Chikianian,⁴⁹ H.A. Choi,³³ W. Christie,⁴ J.P. Coffin,¹⁸ T.M. Cormier,⁴⁷ M.R. Cosentino,³⁶ J.G. Cramer,⁴⁶ H.J. Crawford,⁶ D. Das,⁴⁴ S. Das,⁴⁴ M. Daugherty,⁴¹ M.M. de Moura,³⁶ T.G. Dedovich,¹² M. DePhillips,⁴ A.A. Derevschikov,³¹ L. Didenko,⁴ T. Dietel,¹⁴ S.M. Dogra,¹⁹ W.J. Dong,⁸ X. Dong,³⁷ J.E. Draper,⁷ F. Du,⁴⁹ A.K. Dubey,¹⁵ V.B. Dunin,¹² J.C. Dunlop,⁴ M.R. Dutta Mazumdar,⁴⁴ V. Eckardt,²³ W.R. Edwards,²¹ L.G. Efimov,¹² V. Emelianov,²⁵ J. Engelage,⁶ G. Eppley,³⁵ B. Erazmus,³⁹ M. Estienne,³⁹ P. Fachini,⁴ J. Faivre,¹⁸ R. Fatemi,²² J. Fedorisin,¹² K. Filimonov,²¹ P. Filip,¹¹ E. Finch,⁴⁹ V. Fine,⁴ Y. Fisyak,⁴ K.S.F. Fornazier,³⁶ J. Fu,⁴² C.A. Gagliardi,⁴⁰ L. Gaillard,³ J. Gans,⁴⁹ M.S. Ganti,⁴⁴ F. Geurts,³⁵ V. Ghazikhanian,⁸ P. Ghosh,⁴⁴ J.E. Gonzalez,⁸ H. Gos,⁴⁵ O. Grachov,⁴⁷ O. Grebenyuk,²⁷ D. Grosnick,⁴³ S.M. Guerten,⁸ Y. Guo,⁴⁷ A. Gupta,¹⁹ N. Gupta,¹⁹ T.D. Gutierrez,⁷ T.J. Hallman,⁴ A. Hamed,⁴⁷ D. Hardtke,²¹ J.W. Harris,⁴⁹ M. Heinz,² T.W. Henry,⁴⁰ S. Hepplemann,³⁰ B. Hippolyte,¹⁸ A. Hirsch,³² E. Hjort,²¹ G.W. Hoffmann,⁴¹ M.J. Horner,²¹ H.Z. Huang,⁸ S.L. Huang,³⁷ E.W. Hughes,⁵ T.J. Humanic,²⁸ G. Igo,⁸ A. Ishihara,⁴¹ P. Jacobs,²¹ W.W. Jacobs,¹⁷ M. Jedynak,⁴⁵ H. Jiang,⁸ P.G. Jones,³ E.G. Judd,⁶ S. Kabana,² K. Kang,⁴² M. Kaplan,⁹ D. Keane,²⁰ A. Kechechyan,¹² V.Yu. Khodyrev,³¹ B.C. Kim,³³ J. Kiryluk,²² A. Kisiel,⁴⁵ E.M. Kislov,¹² J. Klay,²¹ S.R. Klein,²¹ D.D. Koetke,⁴³ T. Kollegger,¹⁴ M. Kopytine,²⁰ L. Kotchenda,²⁵ K.L. Kowalik,²¹ M. Kramer,²⁶ P. Kravtsov,²⁵ V.I. Kravtsov,³¹ K. Krueger,¹ C. Kuhn,¹⁸ A.I. Kulikov,¹² A. Kumar,²⁹ R.Kh. Kutuev,¹³ A.A. Kuznetsov,¹² M.A.C. Lamont,⁴⁹ J.M. Landgraf,⁴ S. Lange,¹⁴ F. Laue,⁴ J. Lauret,⁴ A. Lebedev,⁴ R. Lednický,¹² C-H. Lee,³³ S. Lehocka,¹² M.J. LeVine,⁴ C. Li,³⁷ Q. Li,⁴⁷ Y. Li,⁴² G. Lin,⁴⁹ S.J. Lindenbaum,²⁶ M.A. Lisa,²⁸ F. Liu,⁴⁸ H. Liu,³⁷ J. Liu,³⁵ L. Liu,⁴⁸ Q.J. Liu,⁴⁶ Z. Liu,⁴⁸ T. Ljubicic,⁴ W.J. Llope,³⁵ H. Long,⁸ R.S. Longacre,⁴ M. Lopez-Noriega,²⁸ W.A. Love,⁴ Y. Lu,⁴⁸ T. Ludlam,⁴ D. Lynn,⁴ G.L. Ma,³⁸ J.G. Ma,⁸ Y.G. Ma,³⁸ D. Magestro,²⁸ S. Mahajan,¹⁹ D.P. Mahapatra,¹⁵ R. Majka,⁴⁹ L.K. Mangotra,¹⁹ R. Manweiler,⁴³ S. Margetis,²⁰ C. Markert,²⁰ L. Martin,³⁹ J.N. Marx,²¹ H.S. Matis,²¹ Yu.A. Matulenko,³¹ C.J. McClain,¹ T.S. McShane,¹⁰ F. Meissner,²¹ Yu. Melnick,³¹ A. Meschanin,³¹ M.L. Miller,²² N.G. Minaev,³¹ C. Mironov,²⁰ A. Mischke,²⁷ D.K. Mishra,¹⁵ J. Mitchell,³⁵ B. Mohanty,⁴⁴ L. Molnar,³² C.F. Moore,⁴¹ D.A. Morozov,³¹ M.G. Munhoz,³⁶ B.K. Nandi,⁴⁴ S.K. Nayak,¹⁹ T.K. Nayak,⁴⁴ J.M. Nelson,³ P.K. Netrakanti,⁴⁴ V.A. Nikitin,¹³ L.V. Nogach,³¹ S.B. Nurushev,³¹ G. Odyniec,²¹ A. Ogawa,⁴ V. Okorokov,²⁵ M. Oldenburg,²¹ D. Olson,²¹ S.K. Pal,⁴⁴ Y. Panebratsev,¹² S.Y. Panitkin,⁴ A.I. Pavlinov,⁴⁷ T. Pawlak,⁴⁵ T. Peitzmann,²⁷ V. Perevozchikov,⁴ C. Perkins,⁶ W. Peryt,⁴⁵ V.A. Petrov,⁴⁷ S.C. Phatak,¹⁵ R. Picha,⁷ M. Planinic,⁵⁰ J. Pluta,⁴⁵ N. Porile,³² J. Porter,⁴⁶ A.M. Poskanzer,²¹ M. Potekhin,⁴ E. Potrebenikova,¹² B.V.K.S. Potukuchi,¹⁹ D. Prindle,⁴⁶ C. Pruneau,⁴⁷ J. Putschke,²¹ G. Rakness,³⁰ R. Raniwala,³⁴ S. Raniwala,³⁴ O. Ravel,³⁹ R.L. Ray,⁴¹ S.V. Razin,¹² D. Reichhold,³² J.G. Reid,⁴⁶ J. Reinnarth,³⁹ G. Renault,³⁹ F. Retiere,²¹ A. Ridiger,²⁵ H.G. Ritter,²¹ J.B. Roberts,³⁵ O.V. Rogachevskiy,¹² J.L. Romero,⁷ A. Rose,²¹ C. Roy,³⁹ L. Ruan,³⁷ M.J. Russcher,²⁷ R. Sahoo,¹⁵ I. Sakrejda,²¹ S. Salur,⁴⁹ J. Sandweiss,⁴⁹ M. Sarsour,¹⁷ I. Savin,¹³ P.S. Sazhin,¹² J. Schambach,⁴¹ R.P. Scharenberg,³² N. Schmitz,²³ K. Schweda,²¹ J. Seger,¹⁰ P. Seyboth,²³ E. Shahaliev,¹² M. Shao,³⁷ W. Shao,⁵ M. Sharma,²⁹ W.Q. Shen,³⁸ K.E. Shestermanov,³¹ S.S. Shimanskiy,¹² E. Sichtermann,²¹ F. Simon,²² R.N. Singaraju,⁴⁴ N. Smirnov,⁴⁹ R. Snellings,²⁷ G. Sood,⁴³ P. Sorensen,²¹ J. Sowinski,¹⁷ J. Speltz,¹⁸ H.M. Spinka,¹ B. Srivastava,³² A. Stadnik,¹² T.D.S. Stanislaus,⁴³ R. Stock,¹⁴ A. Stolpovsky,⁴⁷ M. Strikhanov,²⁵ B. Stringfellow,³² A.A.P. Suade,³⁶ E. Sugarbaker,²⁸ M. Sumbera,¹¹ B. Surrow,²² M. Swanger,¹⁰ T.J.M. Symons,²¹ A. Szanto de Toledo,³⁶ A. Tai,⁸ J. Takahashi,³⁶ A.H. Tang,²⁷ T. Tarnowsky,³² D. Thein,⁸ J.H. Thomas,²¹ A.R. Timmins,³ S. Timoshenko,²⁵ M. Tokarev,¹² T.A. Trainor,⁴⁶ S. Trentalange,⁸ R.E. Tribble,⁴⁰ O.D. Tsai,⁸ J. Ulery,³² T. Ullrich,⁴ D.G. Underwood,¹ G. Van Buren,⁴ N. van der Kolk,²⁷ M. van Leeuwen,²¹ A.M. Vander Molen,²⁴ R. Varma,¹⁶ I.M. Vasilevski,¹³ A.N. Vasiliev,³¹ R. Vernet,¹⁸ S.E. Vigdor,¹⁷ Y.P. Viyogi,⁴⁴ S. Vokal,¹² S.A. Voloshin,⁴⁷ W.T. Waggoner,¹⁰ F. Wang,³² G. Wang,²⁰ G. Wang,⁵ X.L. Wang,³⁷ Y. Wang,⁴¹ Y. Wang,⁴² Z.M. Wang,³⁷ H. Ward,⁴¹ J.W. Watson,²⁰ J.C. Webb,¹⁷ G.D. Westfall,²⁴ A. Wetzler,²¹ C. Whitten Jr.,⁸ H. Wieman,²¹ S.W. Wissink,¹⁷ R. Witt,² J. Wood,⁸ J. Wu,³⁷ N. Xu,²¹ Z. Xu,⁴ Z.Z. Xu,³⁷

E. Yamamoto,²¹ P. Yepes,³⁵ I-K. Yoo,³³ V.I. Yurevich,¹² I. Zborovsky,¹¹ H. Zhang,⁴ W.M. Zhang,²⁰ Y. Zhang,³⁷ Z.P. Zhang,³⁷ C. Zhong,³⁸ R. Zoukarneev,¹³ Y. Zoukarneeva,¹³ A.N. Zubarev,¹² and J.X. Zuo³⁸
(STAR Collaboration)

¹Argonne National Laboratory, Argonne, Illinois 60439

²University of Bern, 3012 Bern, Switzerland

³University of Birmingham, Birmingham, United Kingdom

⁴Brookhaven National Laboratory, Upton, New York 11973

⁵California Institute of Technology, Pasadena, California 91125

⁶University of California, Berkeley, California 94720

⁷University of California, Davis, California 95616

⁸University of California, Los Angeles, California 90095

⁹Carnegie Mellon University, Pittsburgh, Pennsylvania 15213

¹⁰Creighton University, Omaha, Nebraska 68178

¹¹Nuclear Physics Institute AS CR, 250 68 Řež/Prague, Czech Republic

¹²Laboratory for High Energy (JINR), Dubna, Russia

¹³Particle Physics Laboratory (JINR), Dubna, Russia

¹⁴University of Frankfurt, Frankfurt, Germany

¹⁵Institute of Physics, Bhubaneswar 751005, India

¹⁶Indian Institute of Technology, Mumbai, India

¹⁷Indiana University, Bloomington, Indiana 47408

¹⁸Institut de Recherches Subatomiques, Strasbourg, France

¹⁹University of Jammu, Jammu 180001, India

²⁰Kent State University, Kent, Ohio 44242

²¹Lawrence Berkeley National Laboratory, Berkeley, California 94720

²²Massachusetts Institute of Technology, Cambridge, MA 02139-4307

²³Max-Planck-Institut für Physik, Munich, Germany

²⁴Michigan State University, East Lansing, Michigan 48824

²⁵Moscow Engineering Physics Institute, Moscow Russia

²⁶City College of New York, New York City, New York 10031

²⁷NIKHEF and Utrecht University, Amsterdam, The Netherlands

²⁸Ohio State University, Columbus, Ohio 43210

²⁹Panjab University, Chandigarh 160014, India

³⁰Pennsylvania State University, University Park, Pennsylvania 16802

³¹Institute of High Energy Physics, Protvino, Russia

³²Purdue University, West Lafayette, Indiana 47907

³³Pusan National University, Pusan, Republic of Korea

³⁴University of Rajasthan, Jaipur 302004, India

³⁵Rice University, Houston, Texas 77251

³⁶Universidade de São Paulo, São Paulo, Brazil

³⁷University of Science & Technology of China, Anhui 230027, China

³⁸Shanghai Institute of Applied Physics, Shanghai 201800, China

³⁹SUBATECH, Nantes, France

⁴⁰Texas A&M University, College Station, Texas 77843

⁴¹University of Texas, Austin, Texas 78712

⁴²Tsinghua University, Beijing 100084, China

⁴³Valparaiso University, Valparaiso, Indiana 46383

⁴⁴Variable Energy Cyclotron Centre, Kolkata 700064, India

⁴⁵Warsaw University of Technology, Warsaw, Poland

⁴⁶University of Washington, Seattle, Washington 98195

⁴⁷Wayne State University, Detroit, Michigan 48201

⁴⁸Institute of Particle Physics, CCNU (HZNU), Wuhan 430079, China

⁴⁹Yale University, New Haven, Connecticut 06520

⁵⁰University of Zagreb, Zagreb, HR-10002, Croatia

(Dated: December 2, 2024)

The first measurements of two-particle correlations on transverse momentum p_t for Au-Au collisions at $\sqrt{s_{NN}} = 130$ GeV are presented. Significant large-momentum-scale correlations are observed for charged primary hadrons with $0.15 \leq p_t \leq 2$ GeV/c and pseudorapidity $|\eta| \leq 1.3$. Such correlations were not observed in a similar study at lower energy and are not predicted by theoretical collision models. Their direct relation to mean- p_t fluctuations measured in the same angular acceptance is demonstrated. The observed correlations are consistent with a scenario in which initial-state semi-hard parton scattering and fragmentation are modified by in-medium dissipation.

I. INTRODUCTION

Correlations and fluctuations can provide essential information about the medium produced in ultrarelativistic heavy ion collisions [1, 2, 3]. *In-medium modification* of parton scattering and fragmentation of energetic partons and the bulk medium can be studied with large-momentum-scale correlations (LSC). In particular, effects of a dissipative medium on parton fragmentation and conversely effects of parton dissipation on the medium are of considerable current interest. Studies of medium modification of jet angular correlations were presented in separate analyses [4, 5]. Alternatively, in this work measurement of two-particle correlations on transverse momentum p_t are presented which may reveal the transition in A-A collisions from *in vacuo* fragmentation functions on p_t to local temperature variations in a partially-equilibrated QCD medium.

Substantial nonstatistical fluctuations in event-wise mean transverse momentum $\langle p_t \rangle$ of charged particles from Au-Au collisions were reported by the STAR [6] and PHENIX [7] experiments at the Relativistic Heavy Ion Collider (RHIC). $\langle p_t \rangle$ fluctuations at RHIC are much larger than those reported at the CERN Super Proton Synchrotron (SPS) with one-tenth the CM energy [8], and were not predicted by theoretical models [6, 9, 10, 11]. $\langle p_t \rangle$ fluctuations could result from several dynamical processes including incompletely-equilibrated initial-state multiple scattering (ISS) [12] or minijet production [9] where the increased hard-scattering cross section at RHIC energies produces greater two-particle p_t correlations there. $\langle p_t \rangle$ fluctuations can be directly related to number correlations on p_t . The latter, by providing differential information, may better reveal the underlying dynamics.

In this Letter we report the first measurements of two-particle number correlations on transverse momentum p_t at RHIC based on $\sqrt{s_{NN}} = 130$ GeV Au-Au collisions observed with the STAR detector [13]. The observed correlations are consistent with semi-hard parton scattering and fragmentation modified by dissipation in a dense medium and were not anticipated by theory.

II. ANALYSIS METHOD

Our goal is to determine the complete *charge-independent* (CI) correlation structure of charged hadron pair density $\rho(\vec{p}_1, \vec{p}_2)$ *without imposing a correlation model*. In other analyses the full two-particle momentum space was projected onto pseudorapidity and azimuth *angular* subspace $(\eta_1, \eta_2, \phi_1, \phi_2)$ and in turn onto the two-dimensional (2D) subspace of angular difference variables $(\eta_1 - \eta_2, \phi_1 - \phi_2)$ by integrating over a specific transverse momentum interval [4, 14]. In the present analysis

the complementary correlation structure on two-particle transverse momentum space (p_{t1}, p_{t2}) is determined by integrating over a specific detector angular acceptance.

Differential analysis is achieved by comparing object distribution ρ_{sib} of pairs taken from single events (sibling pairs) with reference distribution ρ_{mix} of pairs where the particles in the pair are taken from different but similar events (mixed pairs). The correlation function and pair-density ratio used here are defined by

$$C(\vec{p}_1, \vec{p}_2) = \rho_{sib}(\vec{p}_1, \vec{p}_2) - \rho_{mix}(\vec{p}_1, \vec{p}_2) \\ r(\vec{p}_1, \vec{p}_2) \equiv \rho_{sib}(\vec{p}_1, \vec{p}_2)/\rho_{mix}(\vec{p}_1, \vec{p}_2). \quad (1)$$

Pair densities $\rho(\vec{p}_1, \vec{p}_2)$ are not projected onto subspace (p_{t1}, p_{t2}) with strongly-varying pair density, but rather onto nonuniform p_t bins defined by the binned space $[X(p_{t1}), X(p_{t2})]$ constructed to provide nearly uniform statistical precision over the p_t acceptance used here from 0.15 to 2.0 GeV/c, with quantity $X(p_t) \equiv 1 - \exp\{-(m_t - m_\pi)/0.4 \text{ GeV}\} \in [0, 1]$ ($m_t = \sqrt{p_t^2 + m_\pi^2}$, pion mass m_π assumed) and with uniform X bin size 1/25 [15].

Resulting histograms $n_{ab} \simeq 1/25^2 \rho(X_a, X_b)$ (ab are 2D bin indices) for sibling and mixed pairs are separately normalized to the total number of detected pairs in each event class $\hat{n}_{ab} = n_{ab}/\sum_{ab} n_{ab}$. Normalized pair-number ratios $\hat{r}_{ab} = \hat{n}_{ab,sib}/\hat{n}_{ab,mix}$ are the basis for this analysis. Ratios are formed for subsets of events with similar centrality (multiplicities differ by ≤ 100 , except ≤ 50 for most-central) and primary-vertex location (within 7.5 cm along the beam axis) and combined as weighted (by sibling pair number) averages within each centrality class.

Deviations of event-wise $\langle p_t \rangle$ fluctuations from a central-limit-theorem reference [16, 17] are measured by scale-dependent variance difference $\Delta\sigma_{p_t:n}^2$ introduced in [6], where it was evaluated at the STAR detector acceptance scale (bin size). $\Delta\sigma_{p_t:n}^2$ can be expressed as a *weighted integral* on (p_{t1}, p_{t2}) of pair-density difference $\rho_{sib} - \rho_{mix}$. It can be rewritten exactly as a discrete sum over p_t products [16], the sum approximated in turn by the weighted integral

$$\Delta\sigma_{p_t:n}^2 \equiv \frac{1}{N} \frac{1}{\epsilon} \sum_{j=1}^{\epsilon} \sum_{i \neq i'=1}^{N_j} (p_{tji} p_{tji'} - \hat{p}_t^2) \\ = \frac{1}{N} \int \int dp_{t1} dp_{t2} p_{t1} p_{t2} (\rho_{sib} - \rho_{mix}) \\ \equiv \hat{p}_t^2 \bar{N} \langle r(p_{t1}, p_{t2}) - 1 \rangle, \quad (2)$$

where the integral of ρ_{mix} is $\bar{N}^2 \hat{p}_t^2$. N_j is the event-wise number of accepted particles, \bar{N} is the mean event multiplicity in the acceptance, ϵ is the event number, j the event index, \hat{p}_t is the mean of the ensemble-average p_t distribution (all accepted particles from all events in a centrality bin), and i, i' are particle indices. Angle brackets in the last line denote a weighted average with weight $p_{t1} p_{t2} \rho_{mix}(p_{t1}, p_{t2})$. In the present analysis we measure

normalized pair-ratio distributions $\hat{r}[X(p_{t1}), X(p_{t2})]$ exhibiting two-particle number correlations on p_t which correspond to excess $\langle p_t \rangle$ fluctuations. In the following sections it is shown that correlations on $[X(p_{t1}), X(p_{t2})]$ include a saddle shape structure which can be modeled with a 2D *Lévy distribution* representing particles emitted from a source with event-wise and/or spatially varying temperature.

III. DATA

Data for this analysis were obtained with the STAR detector [13] using a 0.25 T uniform magnetic field parallel to the beam axis. Event triggering and charged-particle measurements with the time projection chamber (TPC) are described in [13]. Track definitions, tracking efficiencies, quality cuts and primary-particle definition are described in [6, 18]. Tracks were accepted in $|\eta| \leq 1.3$, $0.15 \leq p_t \leq 2$ GeV/c and 2π azimuth. Particle identification was not implemented. Corrections were made to \hat{r} for two-track inefficiencies due to track merging and intersecting trajectories reconstructed as > 2 particles (splitting) [19]. Small-scale correlations (SSC) (low- $X(p_t)$ peaks), attributed to quantum correlations (HBT) and Coulomb interactions based on MC simulations [20, 21], were removed by discarding sibling and mixed pairs ($\sim 3\%$ of total) with $|\eta_1 - \eta_2| < 0.3$, $|\phi_1 - \phi_2| < \pi/6$ (azimuth), $|p_{t1} - p_{t2}| < 0.15$ GeV/c, if $p_t < 0.8$ GeV/c for either particle. These pair cuts negligibly affect the LSC studied here. Four centrality classes for 300k events labeled (a) - (d) for central to peripheral collisions were defined by cuts on multiplicity N within the acceptance relative to multiplicity end-point N_0 [22], corresponding to the maximum participant number [6]. The four classes were defined by (d) $0.03 < N/N_0 \leq 0.21$, (c) $0.21 < N/N_0 \leq 0.56$, (b) $0.56 < N/N_0 \leq 0.79$ and (a) $N/N_0 > 0.79$, corresponding respectively to fraction of total cross section ranges 40-70%, 17-40%, 5-17% and 0-5%.

IV. TWO-PARTICLE DISTRIBUTIONS

The centrality dependence of quantity $\hat{r} - 1$ is shown in Fig. 1 for four centrality classes. This *per-pair* correlation measure contains a trivial *dilution factor* $1/\bar{N}$ and is therefore numerically a few *permil* for central Au-Au collisions (but greatly exceeds statistical errors) [14]. The $1/\bar{N}$ dilution is removed by adding factor \bar{N} to the model-fit amplitudes as discussed below. The dominant features in Fig. 1 are 1) a large-momentum-scale correlation ‘saddle’ structure with positive (negative) curvature along the $X(p_t)_\Sigma(\Delta) \equiv X(p_{t1}) + (-)X(p_{t2})$ sum (difference) direction from $[X(p_{t1}), X(p_{t2})]$ (0,0) to (1,1) [(0,1) to (1,0)] and 2) a narrow peak structure at large $X(p_t)$ ($p_t > 0.6$ GeV/c). With increasing centrality the negative curvature of the LSC saddle along the difference

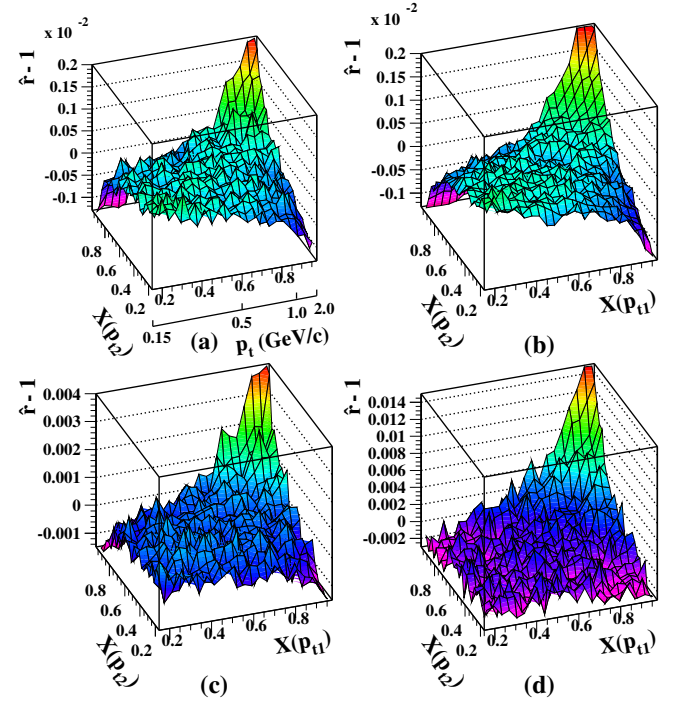


FIG. 1: Symmetrized pair-density net ratios $\hat{r}[X(p_{t1}), X(p_{t2})] - 1$ for all nonidentified charged primary particles for (a) most-central, (b) mid-central, (c) mid-peripheral, and (d) peripheral Au-Au collision events. Note scale change for panels (c) and (d) and auxiliary p_t scale in units GeV/c. SSC were removed (see text). Errors are discussed in Sec. IV.

variable increases in magnitude, the positive curvature along the sum variable decreases, and the magnitude of the peak at large $X(p_t)$ also decreases. The same analysis applied to Pb-Pb collisions in $1.1 < y_{cm} < 2.6$ at the CERN SPS did not reveal any statistically significant CI correlations [23] when SSC (see Sec. III) were removed with pair cuts. The analysis in [24] of proton + proton and various nucleus + nucleus collision data from the CERN SPS for $1.1 < y_{cm} < 2.6$ without those pair cuts revealed SSC peaks at low $X(p_t)$ along the $X(p_t)_\Sigma$ direction.

Per-bin statistical errors for $\hat{r} - 1$ in Fig. 1 range from ~ 6 -9% of the maximum correlation amplitude for each centrality (typically 0.00015, 0.00011, 0.00035 and 0.001 for centralities (a)-(d) respectively). Systematic errors [6] are dominated by contamination from non-primary background particles, mainly weak-decay daughters [18]. Correlations between the latter and true primary particles were assumed to vary from zero to the same correlation amplitude as primary particles. Conversion electron contamination is suppressed by the lower p_t acceptance cut and also by the pair cuts described in Sec. III. Multiplicative corrections (not applied in Fig. 1) and total systematic errors for $\hat{r} - 1$ were obtained from the average and half difference of these two limiting cases and varied respectively from 1.07 and $\pm 7\%$ for $X(p_{t1,2}) > 0.4$ up to

1.16 and $\pm 16\%$ for $X(p_{t1,2}) < 0.4$ and 1.12 and $\pm 12\%$ in the off-diagonal corners [*i.e.*, near (0,1) and (1,0)]. Resonance (ρ^0, ω) decay daughters were estimated [21] to contribute a small saddle-shape correlation with curvature opposite to the data and amplitude at the corners approximately 0.0002 for the most-central data, increasing as $1/\bar{N}$ for the remaining centrality bins.

V. ONE- AND TWO-DIMENSIONAL LÉVY DISTRIBUTIONS

The features of the data in Fig. 1 can be described by two limiting cases: 1) a saddle shape which may represent local gaussian temperature and/or collective velocity fluctuations of the bulk medium on (η, ϕ) and 2) a large- $X(p_t)$ peak which may represent fragmenting partons as observed in p-p collisions at RHIC [25]. Final-state hadrons from heavy ion collisions sample *local* event-wise parent p_t distributions representing a complex particle source (the bulk medium plus partially dissipated partons) with an event-wise varying velocity/temperature distribution on (η, ϕ) .

The composite source is modeled with an event-wise dependence on (η, ϕ) of m_t spectrum shape parameter $\beta = 1/T$ or v/c . A fully-equilibrated source would be described by global effective temperature parameter $\beta_0 \equiv 1/T_0$. If a source is *partially* equilibrated, the local velocity/temperature distribution can be represented by *event-wise changing* function $\beta(\eta, \phi)$ [*e.g.*, as local temperature fluctuations occurring randomly on (η, ϕ)] determining the shapes of the effective local-parent m_t spectra sampled by final-state hadrons. Each final-state hadron therefore samples an event-wise $\beta(\eta, \phi)$. If the distribution of sampled β values over an event ensemble is represented by peaked distribution $g_1(\beta)$, with centroid β_0 and variance σ_β^2 , the ensemble-average m_t spectrum is given by convoluting thermal spectrum $e^{-\beta(m_t - m_\pi)}$ with $g_1(\beta)$. For example, if $g_1(\beta)$ is a gamma distribution [26] then $1/m_t dN/dm_t$ can be conveniently represented by the resulting one-dimensional (1D) Lévy distribution [27] $A/\{1 + \beta_0(m_t - m_\pi)/n\}^n$. Inverse exponent $1/n \equiv \sigma_\beta^2/\beta_0^2$ is the *relative variance* of $g_1(\beta)$. We emphasize that any finite-width peaked function $g_1(\beta)$ results in an m_t distribution which decreases less rapidly with increasing m_t than thermal spectrum $e^{-\beta_0 m_t}$. Deviations of the observed m_t distribution from a thermal spectrum, as measured by exponent n , are expected from transverse expansion and hard partonic scattering, but in addition are affected by local $\beta(\eta, \phi)$ (temperature/velocity) fluctuations if present. Consequently, fitting $1/m_t dN/dm_t$ spectra to obtain n cannot by itself determine the degree of equilibration.

Within this model the shape of two-particle number correlations on m_t is determined by the average *two-point* structure of $\beta(\eta, \phi)$. This can be understood as follows. Final-state hadron pairs sample two-particle local-parent spectra $e^{-\beta_1(m_{t1} - m_\pi)}e^{-\beta_2(m_{t2} - m_\pi)}$ with the

event-ensemble distribution of (β_1, β_2) pairs represented by 2D function $g_2(\beta_1, \beta_2)$. For uncorrelated β fluctuations or for mixed pairs, g_2 factorizes as $g_2(\beta_1, \beta_2) = g_1(\beta_1) \cdot g_1(\beta_2)$, implying zero covariance. For *global* fluctuations (event-wise-uniform β) $g_2(\beta_1, \beta_2) \propto g'_1(\beta_1)\delta(\beta_1 - \beta_2)$, a diagonal locus with maximum covariance. The second scenario represents the conventional picture of an ensemble of equilibrated events with ‘event-by-event’ fluctuations in the global temperature. In general, the observed two-particle (m_{t1}, m_{t2}) spectrum is the convolution of thermal spectrum $e^{-\beta_1(m_{t1} - m_\pi)}e^{-\beta_2(m_{t2} - m_\pi)}$ with $g_2(\beta_1, \beta_2)$. If $g_2(\beta_1, \beta_2)$ is represented by a 2D gamma distribution the two-particle (m_{t1}, m_{t2}) spectrum can be conveniently described by an analytic 2D Lévy distribution

$$F_{sib} \propto \left(1 + \frac{\beta_0 m_{t\Sigma}}{2n_\Sigma}\right)^{-2n_\Sigma} \left[1 - \left(\frac{\beta_0 m_{t\Delta}}{2n_\Delta + \beta_0 m_{t\Sigma}}\right)^2\right]^{-n_\Delta} \quad (3)$$

on sum and difference variables $m_{t\Sigma} \equiv m_{t1} + m_{t2} - 2m_\pi$ and $m_{t\Delta} \equiv m_{t1} - m_{t2}$. Inverse exponents $1/n_\Sigma$ and $1/n_\Delta$ are the relative variances of $g_2(\beta_1, \beta_2)$ along sum and difference variables β_Σ and β_Δ respectively, and $\Delta(1/n)_{tot} \equiv 1/n_\Sigma - 1/n_\Delta$ is the relative *covariance* of g_2 [28], measuring velocity/temperature correlations. Mixed-pair distribution $F_{mix}(p_{t1}, p_{t2})$, a product of 1D Lévy distributions, has the form of Eq. (3) but with $n_\Sigma = n_\Delta = n$. Ratio $r_{model} \equiv F_{sib}/F_{mix}$ is therefore based on a phenomenological velocity/temperature fluctuation model which can be tested by comparison to the data in Fig. 1 via chi-square fits. We emphasize for this 2D case that any peaked function $g_2(\beta_1, \beta_2)$ with *nonzero covariance* results in a 2D saddle shape distribution for r_{model} . Relative variance *differences* $\Delta(1/n)_\Sigma \equiv (1/n_\Sigma - 1/n)$ and $\Delta(1/n)_\Delta \equiv (1/n_\Delta - 1/n)$ measure the *saddle curvatures* of r_{model} (and hence the data) along sum and difference directions at the origin, which these fits best determine.

VI. ANALYTICAL MODEL FITS

Data in Fig. 1 (excluding peak region $X(p_t)_\Sigma > 1.6$) were fitted with $r_{model} - 1 + \mathcal{C}$ by varying parameters n_Σ , n_Δ and \mathcal{C} (offset). Parameter $\beta_0 = 5 \text{ GeV}^{-1}$ was fixed by the ensemble-mean p_t spectrum for $p_t < 1 \text{ GeV}/c$. The fits are insensitive to the absolute value of $1/n$; its value was fixed as follows. Parameter $1/n$ accounts for the deviation between the measured m_t distribution and $e^{-\beta_0 m_t}$, reflecting the effects of transverse expansion (radial flow) and velocity/temperature fluctuations (including hard scattering). The two contributions can be written as $1/n = 1/n_{flow} + 1/n_{fluct}$. Since component $1/n_{fluct}$ relevant to the Lévy saddle fit is not accessible, fits to 2D $\hat{r} - 1$ distributions can only weakly constrain absolute quantities $1/n_\Sigma$ and $1/n_\Delta$. However, *differences* $\Delta(1/n)_{\Sigma, \Delta}$ are well determined by the saddle curvatures, nearly independently of $1/n \rightarrow 1/n_{fluct}$. A

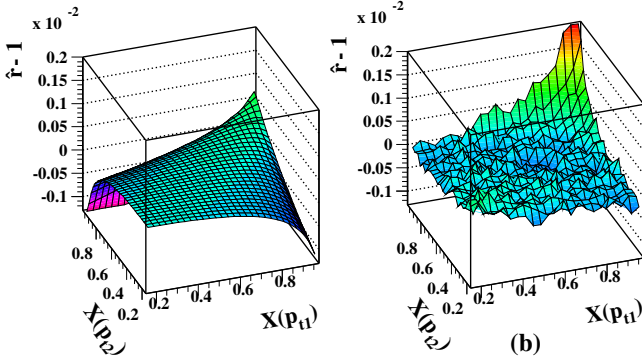


FIG. 2: Left: pair-density net ratio $r_{model}[X(p_t1), X(p_t2)] - 1$ for model fit to mid-central (b) Au-Au collisions. Right: residuals (data – model) for mid-central collisions.

value $1/n_{fluct} = 0.03$ near the center of the allowed range $1/13$ [18] (maximum value if $1/n_{flow} = 0$) to 0.0012 (minimum value necessary to account for $\Delta(1/n)_{tot}$ in Table I) provided stable $\Delta(1/n)_\Sigma$ and $\Delta(1/n)_\Delta$ fit values. Best-fit parameters and χ^2/DoF for the saddle fits are listed in Table I. The model function and residuals for the fit to centrality (b) are shown in Fig. 2.

TABLE I: Parameters and fitting errors (only) for 2D velocity/temperature fluctuation model for each centrality bin, (a) - (d) (central - peripheral as in Fig. 1). Errors (last column) represent fitting uncertainties. Systematic errors are 7-12% [29]. Extrapolation factors \mathcal{S} (last row) correct for contamination and tracking inefficiency [6].

centrality	(d)	(c)	(b)	(a)	error ^a (%)
\bar{N}	115.5	424.9	790.2	983.0	
$C \times 10^4$	-11.6	-0.820	0.787	0.750	6-14
$\Delta(1/n)_\Sigma \times 10^4$	3.54	0.611	0.183	0.118	6-24
$\Delta(1/n)_\Delta \times 10^4$	-8.61	-3.33	-2.53	-2.04	6-3
$\Delta(1/n)_{tot} \times 10^4$	12.2	3.95	2.71	2.16	
χ^2/DoF	$\frac{348}{286}$	$\frac{313}{286}$	$\frac{475}{286}$	$\frac{402}{286}$	
\mathcal{S}	1.19	1.22	1.25	1.27	8^b

^aRange of fitting errors in percent from peripheral to central.

^bSystematic error.

Two-dimensional saddle-fit residuals, as in Fig. 2 (right panel), are independent of difference $X(p_t)_\Delta$: the Lévy temperature fluctuation model adequately describes the saddle structure. Residuals from the fit for mid-central events (b) are shown in Fig. 3 (left panel) projected onto sum variable $X(p_t)_\Sigma$. Errors are included in the data symbols and are smaller than those in Fig. 2 (right panel) due to bin averaging. Residuals for other centralities are similar, but differ in amplitude. We speculate that this residual structure is due to semi-hard parton scattering (minijets) [25]. Centrality dependences on mean participant path length ν [30] of efficiency-corrected *per-particle* model parameters $\mathcal{S}\bar{N}\Delta(1/n)$ [31] (see discussion below), which determine saddle amplitudes in Fig. 1, are shown in Fig. 3 (right panel). The linear trends suggested by the solid lines are notable.

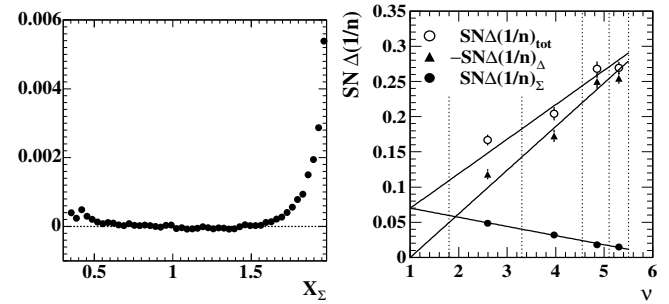


FIG. 3: Left: Residuals from 2D Lévy saddle fit to mid-central (b) data in Fig. 1 projected onto sum variable $X(p_t)_\Sigma$. Right: Efficiency-corrected *per-particle* saddle-curvature measures [31] on centrality ν : $\mathcal{S}\bar{N}\Delta(1/n)_\Sigma$ (dots), $-\mathcal{S}\bar{N}\Delta(1/n)_\Delta$ (triangles) and $\mathcal{S}\bar{N}\Delta(1/n)_{tot}$ (open circles). Data symbols include fitting errors only [29]. Solid lines are linear fits.

VII. MONTE CARLO MODELS

Theoretical and phenomenological model predictions for quantity $\hat{r} - 1$ for central Au-Au collisions at 130 GeV are shown in Fig. 4. HIJING [9] (with jet quenching on - left panel), which models pQCD jet quenching and color-string fragmentation, exhibits significant structure only at high p_t ($X(p_t)_\Sigma > 1.6$) consistent with jet production. The shape is qualitatively different from the 2D Lévy model and data. Although HIJING does model jet quenching, its pQCD model produces no evidence of the saddle structure one might expect from parton dissipation in the QCD medium. RQMD [10], a resonance-gas model, predicts shape and amplitudes for $\hat{r} - 1$ which qualitatively differ from data. Fig. 4 (right panel) shows predictions of a Monte Carlo simulation in which events are produced by sampling average single-particle (p_t, η, ϕ) distributions from data while varying the event-wise inverse slope parameter of the p_t distribution according to a gaussian with $\sigma_T/T_0 = 1.5\%$ [21]. The width was adjusted to approximate the overall amplitude of the data in Fig. 1 (a). Fig. 4 (right panel) shows that this Monte Carlo is consistent with the shape of the saddle feature in the data. Other theoretical models which combine initial-state parton scattering, energy loss, dissipation, rescattering and recombination [11, 32] may eventually explain these correlation data, but relevant predictions are not available at this time.

VIII. DISCUSSION

Correlations on p_t have two main components, a saddle shape and a peak at higher p_t . By measuring the saddle curvatures we infer the relative covariance of two-point distribution $g_2(\beta_1, \beta_2)$ and hence the average two-point correlation amplitude of the temperature/velocity structure of the composite particle source. We now consider possible dynamical origins of that structure.

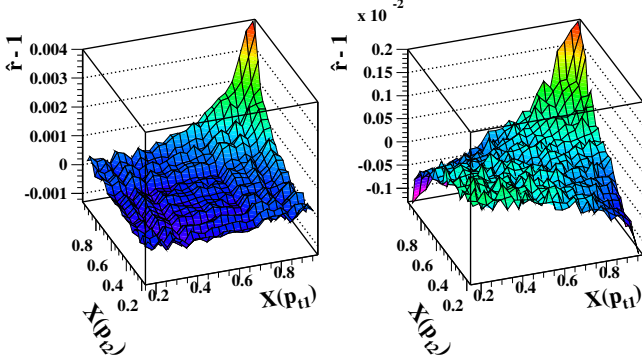


FIG. 4: Symmetrized pair-density ratio $\hat{r}[X(p_{t1}), X(p_{t2})] - 1$ for unidentified charged particles and for central Au-Au collisions. Left panel: Default HIJING [9] with jet quenching, Right panel: a Monte Carlo model [21] which simulates event-wise global temperature fluctuations (see text).

If σ_β^2 were dominated by temperature fluctuations ($\beta \rightarrow 1/T$), the present fixed-scale correlation measurement of saddle curvatures would set a *lower* limit on local temperature fluctuations (or *upper* limit on global fluctuations) $\sigma_\beta/\beta_0 \rightarrow \sigma_T/T_0 \geq \sqrt{\Delta(1/n)_{tot}/2} \sim 1\%$ for central events. The upper limit on local fluctuations $\sigma_T/T_0 \leq \sqrt{1/n} \sim 30\%$ is derived from the ensemble-mean p_t spectrum. An unknown fraction of variance σ_β^2 represents transverse flow; thus, local temperature variation could range between 1 and 30%. One can ask what is the source of the variation, and is local source velocity rather than temperature a more appropriate quantity?

Given the correlations at higher p_t it is reasonable to speculate that the correlation structures in Fig. 1 result from in-medium modification (dissipation) of a two-particle *parton fragment distribution* on (p_{t1}, p_{t2}) . Since no selection was made on parton momentum in A-A collisions we refer to minimum-bias jets or minijets, and consequently to minijet dissipation. Minijet production and subsequent dissipation in A-A collisions should increase linearly with number of binary collisions N_{bin} [33], thus providing a basis for experimental tests of this hypothesis.

A suitable measure for non-trivial centrality dependence can be constructed by considering a naïve model in which A-A collisions are linear superpositions of nucleon-nucleon collisions. Quantity $\hat{r} - 1$, the number of correlated pairs *per final-state pair*, when multiplied by average event multiplicity \bar{N} , is proportional to the number of correlated pairs *per final-state particle* and would be independent of A-A centrality in the case of linear superposition. We therefore multiply curvature parameters in Table I, proportional to the amplitudes of the saddle-shape correlation, by $\mathcal{S}\bar{N}$, where \mathcal{S} is a contamination and tracking inefficiency correction factor given in Table I. If LSC amplitudes for real A-A collisions stem from semi-hard parton scattering and dissipation, which is proportional to N_{bin} , the resulting density of correlated pairs per final-state particle should be pro-

portional to $\nu \simeq 2N_{bin}/N_{part}$ [30], where the final-state multiplicity is approximately proportional to the number of participant nucleons N_{part} . The linear trends in Fig. 3 (right panel) therefore support, but do not *require*, a minijet origin for the observed correlations on p_t . In Fig. 3 we also observe 1) reduced curvature along the sum direction and 2) increased curvature along the difference direction which may represent respectively transport of semi-hard parton structure to lower p_t and a more correlated bulk medium. Given a minijet interpretation of $\mathcal{S}\bar{N}\Delta(1/n)_{tot}$, the combined trends 1) and 2) represent strong evidence for increased parton dissipation in the more central Au-Au collisions. The present results complement the observed suppression of high- p_t spectra (R_{AA}) [33] and suppression of large angle trigger-particle – associated-particle conditional distributions on $\Delta\phi$ [34] in central Au-Au collisions at RHIC. It is very likely that the lower- p_t fluctuations and correlations reported here are, at least in large part, a consequence of the processes which lead to the suppression at higher- p_t .

It is important to note that these correlations on transverse momentum observed at relatively low p_t reveal nominally ‘soft’ structure in relativistic heavy ion collisions which scales with the number of binary collisions N_{bin} , whereas most low- p_t inclusive quantities scale with participant number N_{part} . Binary-collision scaling is conventionally thought to be an aspect of high- p_t physics and initial-state scattering. This analysis suggests that substantial remnants of initial-state parton scattering are present at low p_t in the more central heavy ion collisions.

IX. SUMMARY

In conclusion, the dynamical origins of excess $\langle p_t \rangle$ fluctuations in Au-Au collisions at RHIC are probed in this first analysis of two-particle correlations on (p_{t1}, p_{t2}) . The velocity/temperature structure of heavy ion collisions suggested by these correlations is unanticipated by theoretical models. The observed correlations on (p_{t1}, p_{t2}) may be interpreted as resulting from semi-hard parton scattering and subsequent fragmentation which is strongly modified by in-medium parton dissipation in the more central Au-Au collisions. In this picture, with increasing centrality the two-particle fragment distribution is shifted to lower p_t , asymptotically approaching a form consistent with random velocity/temperature variations (Lévy saddle) as a manifestation of substantial but incomplete equilibration. These newly-observed p_t correlations may thus reveal minijet dissipation in the medium produced by Au-Au collisions at RHIC.

We thank the RHIC Operations Group and RCF at BNL, and the NERSC Center at LBNL for their support. This work was supported in part by the HENP Divisions of the Office of Science of the U.S. DOE; the U.S. NSF; the BMBF of Germany; IN2P3, RA, RPL, and EMN of France; EPSRC of the United Kingdom; FAPESP of Brazil; the Russian Ministry of Science and

Technology; the Ministry of Education and the NNSFC of China; IRP and GA of the Czech Republic, FOM of the Netherlands, DAE, DST, and CSIR of the Govern-

ment of India; Swiss NSF; the Polish State Committee for Scientific Research; STAA of Slovakia, and the Korea Sci. & Eng. Foundation.

[1] R. Stock, Nucl. Phys. **A661** (1999) 282c; H. Heiselberg, Phys. Rep. **351** (2001) 161.

[2] A. Dumitru, R. Pisarski, Phys. Lett. **B504** (2001) 282.

[3] M. Stephanov, K. Rajagopal, E. Shuryak, Phys. Rev. D **60** (1999) 114028.

[4] J. Adams *et al.* (STAR Collaboration), nucl-ex/0411003.

[5] C. Adler *et al.* (STAR Collaboration), Phys. Rev. Lett. **90** (2003) 082302; J. Adams *et al.* (STAR Collaboration), Phys. Rev. Lett. **91** (2003) 072304.

[6] J. Adams *et al.* (STAR Collaboration), Phys. Rev. C **71** (2005) 064906.

[7] S. S. Adler *et al.* (PHENIX Collaboration), Phys. Rev. Lett. **93** (2004) 092301.

[8] H. Appelshäuser *et al.* (NA49 Collaboration), Phys. Lett. **B459** (1999) 679; D. Adamová *et al.* (CERES Collaboration), Nucl. Phys. **A727** (2003) 97.

[9] X.-N. Wang, M. Gyulassy, Phys. Rev. D **44** (1991) 3501.

[10] H. Sorge, H. Stöcker, W. Greiner, Nucl. Phys. **A498** (1989) 567c; Ann. Phys. (N.Y.) **192** (1989) 266.

[11] Z.-W. Lin, C. M. Ko, B.-A. Li, B. Zhang and S. Pal, nucl-th/0411110.

[12] M. Gaździcki, A. Leonidov, G. Roland, Eur. Phys. J. C **6** (1999) 365.

[13] K. H. Ackermann *et al.*, Nucl. Instrum. Meth. A **499** (2003) 624; see other STAR papers in volume A499.

[14] J. Adams *et al.* (STAR Collaboration), nucl-ex/0406035.

[15] Other mappings are possible. For example, in analysis of transverse jets, transverse rapidity $y_t(p_t) \equiv \ln\{(m_t + p_t)/m_0\}$ is optimal for comparing longitudinal and transverse fragment distributions; R. J. Porter and T. A. Trainor (STAR Collaboration), hep-ph/0506172.

[16] T. A. Trainor, hep-ph/0001148; the summation in Eq. (2) includes factor N_j/\bar{N} relative to that in [6].

[17] E. U. Condon and H. Odishaw, *Handbook of Physics*, Second Ed. (McGraw-Hill, New York, 1967), C. Eisenhart and M. Zelen, Chpt. 12, pgs. 1-177, 178.

[18] Related to but not equivalent to the power-law exponent in C. Adler *et al.* (STAR Collaboration), Phys. Rev. Lett. **87** (2001) 112303; *ibid.* **89** (2002) 202301.

[19] Track-pair cuts required ≥ 10 cm mean track separation in the TPC. Crossing tracks with separations at mid-radius < 10 cm (z) and < 30 cm (azimuth) were removed.

[20] C. Adler *et al.* (STAR Collaboration), Phys. Rev. Lett. **87** (2001) 082301.

[21] R. Ray and R. Longacre, nucl-ex/0008009.

[22] N_0 , the half-maximum point at the end of the minimum-bias distribution plotted as $d\sigma/dN^{1/4}$, is an estimator on N for the maximum number of participants; $N_{part}/N_{part,max} \simeq N/N_0$ within 4%.

[23] J. G. Reid, Ph. D. thesis, Univ. of Washington, nucl-ex/0302001.

[24] T. Anticic *et al.* (NA49 Collaboration), Phys. Rev. C **70** (2004) 034902.

[25] R. J. Porter and T. A. Trainor (STAR Collaboration), eprint hep-ph/0406330.

[26] M. J. Tannenbaum, Phys. Lett. **B498** (2001) 29.

[27] G. Wilk and Z. Włodarczyk, Phys. Rev. Lett. **84** (2000) 2770; similar to a ‘power-law’ distribution [18].

[28] In the context of velocity/temperature fluctuations this quantity measures $(\beta_1 - \beta_0)(\beta_2 - \beta_0)/\beta_0^2$, the relative covariance of velocity/temperature fluctuations.

[29] Systematic errors for quantities in Fig. 3 (right panel), due to systematic uncertainties in the data (7-12%) plus background and efficiency corrections (8%), are 11-14%.

[30] ν estimates the mean participant path length as a number of encountered nucleons. For this analysis $\nu \equiv 5.5(N/N_0)^{1/3} \simeq 5.5(N_{part}/N_{part,max})^{1/3} \simeq 2N_{bin}/N_{part}$, based on Glauber-model simulations. N_{part} (N_{bin}) is the number of participants (binary collisions).

[31] Multiplication by $\mathcal{S}\bar{N}$ gives *per-particle*, rather than *per-pair*, correlation amplitudes which better reveal non-trivial centrality dependences for A-A collisions relative to an independent nucleon-nucleon collision superposition hypothesis. For the latter case the rescaled correlation amplitudes would be independent of centrality.

[32] R. Hwa and C. Yang, Phys. Rev. C **66** (2002) 025205.

[33] J. Adams *et al.* (STAR Collaboration), Phys. Rev. Lett. **91** (2003) 172302.

[34] C. Adler *et al.* (STAR Collaboration), Phys. Rev. Lett. **90** (2003) 082302.